Analyst

Accepted Manuscript

ROYAL SOCIETY OF CHEMISTRY

www.rsc.org/analyst

Nanoscale characterization of DNA conformation using dual-color fluorescence axial localization and label-free biosensing

Xirui Zhang, [a] *George G. Daaboul,* [b] *Philipp S. Spuhler,* [a] *David S. Freedman,* [b]

Abdulkadir Yurt, [c] *Sunmin Ahn,* [a] *Oguzhan Avci,* [b] *and M. Selim Ünlü*[*a,b]

a. Department of Biomedical Engineering, Boston University, 44 Cummington Mall, Boston, MA 02215

b. Department of Electrical and Computer Engineering, Boston University, 8 Saint Mary's St., Boston, MA 02215

c. Division of Materials Science and Engineering, Boston University, 15 Saint Mary's St., Brookline, MA 02446

[*]Address correspondence to: selim@bu.edu

ABSTRACT: Quantitative determination of the density and conformation of DNA molecules tethered to the surface can help optimize and understand DNA nanosensors and nanodevices, which use conformational or motional changes of surface-immobilized DNA for detection or actuation. We present an interferometric sensing platform that combines (i) dual-color fluorescence spectroscopy for precise axial co-localization of two fluorophores attached at different nucleotides of surface-immobilized DNA molecules and (ii) independent label-free quantification of biomolecule surface density at the same site. Using this platform, we examined the conformation of DNA molecules immobilized on a three-dimensional polymeric surface and demonstrated simultaneous detection of DNA conformational change and binding in real-time. These results demonstrate that independent quantification of both surface density and molecular nanoscale conformation constitutes a versatile approach for nanoscale solid-biochemical interface investigations and molecular binding assays.

KEYWORDS: Fluorescence vertical sectioning, Surface-immobilized DNA, DNA conformation, Biosensor, Polymeric surface coating

Table of contents entry

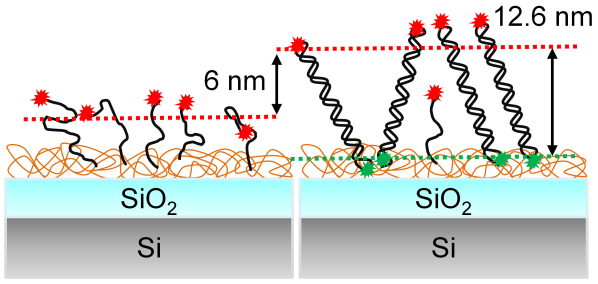

Simultaneous quantification of surface density and conformation of surface-immobilized DNA on a layered substrate functionalized with 3-D polymeric coating.

1. Introduction

The immobilization or synthesis of DNA molecules on a solid surface has stimulated the development of DNA sensors and nanodevices in wide-ranging biomedical applications[1-7]. For instance, DNA microarrays, which allow for massively parallel multiplexed analysis, have become routine for gene-expression profiling in both research and clinical practice[8-10]. In recent years, utilizing surface-immobilized DNA, researchers have developed highly sensitive switching-based biological detectors and dynamic programmable DNA motors[3,6,11-14]. To understand and optimize the sensing and actuation performance of these DNA sensors and nanodevices, it is necessary to characterize two parameters: the DNA surface density and conformation, which dictate the behavior of the surface-immobilized DNA molecules[15-20].

Various optical, electrical, and mechanical techniques have been developed to characterize the surface density, conformation, or thickness of the DNA molecules immobilized on two-dimensional (2-D) functionalized surfaces such as gold, quartz crystal, silicon, silicon dioxide or diamond[21-29]. In recent years, three-dimensional (3-D) polymeric coatings have been commonly used for surface functionalization given their high immobilization specificity and capacity, optimized biological activity, and simple immobilization procedure[30-35]. The axial swelling of the 3-D polymeric coating in aqueous solutions increases the complexity for precise characterization of the biophysical properties of the solution-phase interfacial microenvironment. Here, we report a simple, non-destructive interferometric spectroscopy method to directly determine both the nanoscale conformation and surface density of DNA immobilized on a 3-D polymeric surface.

Spectral self-interference fluorescence microscopy (SSFM) localizes the height of monolayer fluorophores above a reflecting surface from the spectral oscillations caused by the interference between direct and reflected waves of fluorescence emission[36]. SSFM enables the determination

of axial heights of fluorophore tags on surface-immobilized DNA molecules on a two layer SiO_2-Si substrate with subnanometer resolution[36,37]. In this work we have extended SSFM by designing the thickness of the SiO_2 layer to employ two distinct spectral ranges that enables the nanoscale characterization of DNA conformation by determining the average axial height difference between two fluorophore positions on a single DNA spot (Figure 1).

We combined dual-color SSFM with white light reflectance spectroscopy (WLRS) to quantify the DNA surface density to evaluate ensemble conformational measurements (Figure 2). WLRS has been used for label-free detection of bimolecular interactions by monitoring the thickness of the biological layer (bio-layer)[37-39]. The surface density of bound biomolecules can be quantified by calibrating the thickness of the bio-layer to an amount of known deposited biomass and molecular weight[40]. We incorporated WLRS into the dual-color SSFM system by using a light-emitting diode (LED) instead of a white light source traditionally used for illumination, which will be referred to as LED-RS. The interference of the LED light reflected from the top solution/bio-layer interface and that from the bottom SiO_2/Si interface results in spectral oscillations in the collected LED spectrum that shifts upon biomolecule accumulation on the substrate. The emission spectrum of the LED is selected to be distinct from that of the red fluorophores. Thus as shown in Figure 2(b) we can simultaneously measure the bio-layer thickness and the red fluorophore height from a single spectrum measurement. The bio-layer thickness provides information regarding the molecular surface density while the fluorophore heights indicate the conformation of the DNA molecules at the same location on the surface. The capability of SSFM combined with LED-RS to quantify both biomolecule density and conformation is not only desired for the study of specific molecular binding mechanisms[41], but is also needed to characterize the biophysical properties of a biosensing surface[16,42-45].

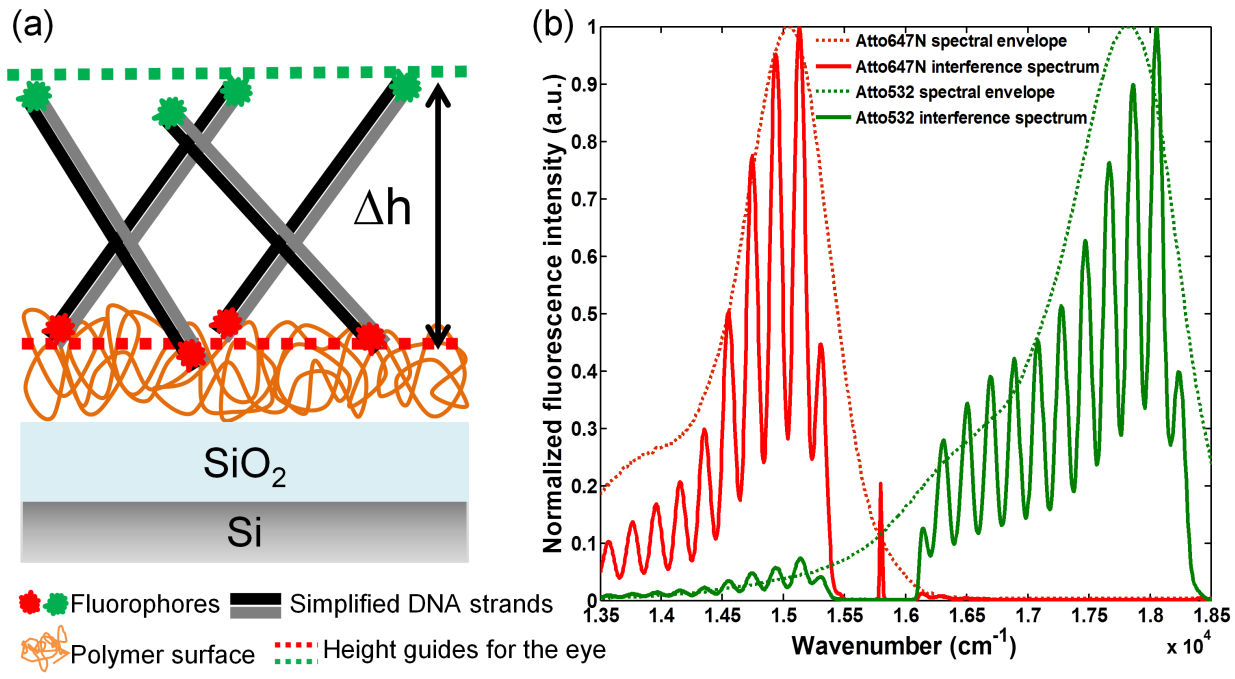

Figure 1. Dual-color SSFM detection principle. (a) Amino-modified DNA molecules labeled with Atto647N (red fluorophores) and Atto532 (green fluorophores) on opposite ends are covalently immobilized on a polymer-functionalized SiO_2-Si substrate. Dual-color SSFM measures the height difference ($\Delta \boldsymbol{h}$) between the DNA surface-distal end (green fluorophores) and the surface-proximal end (red fluorophores). (b) The measured fluorescence interference spectrums of Atto647N and Atto532 on the layered substrate. A few oscillations of each spectrum are fit into an average axial height of the fluorophores to the SiO_2/Si interface with subnanometer accuracy[36]. Dotted lines are the emission spectral envelope of the two fluorophores given by the manufacturer.

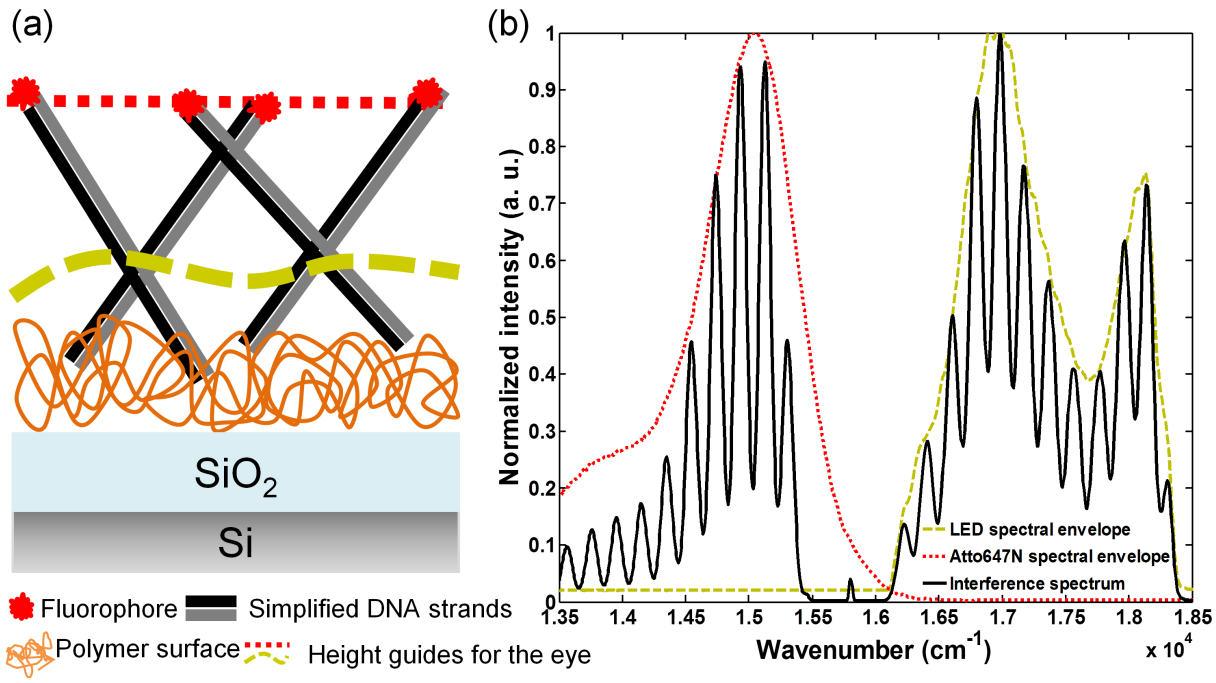

Figure 2. SSFM combined with LED based white light reflectance spectroscopy (referred to as LED-RS). (a) Compare the detection principles of SSFM and LED-RS. Yellow dashed line indicates the thickness of the bio-layer measured by LED-RS while red dotted line indicates the average height of red fluorophores measured by SSFM. (b) Simultaneous acquisition of the average fluorophore axial height and bio-layer thickness. The black line represents the interference spectrum for the LED and the red fluorophores taken from a single acquisition. Yellow dashed line indicates the emission spectral envelope of the LED while the red dotted line is the fluorescence emission spectral envelope of the red fluorophore given by the manufacturer.

2. Experimental

Materials: All buffer solutions were prepared with deionized water (DI water) filtered by Barnstead Nanopure Diamond (18.2 MΩ·cm^{-1}, Thermo Scientific, Waltham, MA). Buffer used for wet measurements was NaCl/Tris solution prepared with Tris buffered saline tablets and NaCl (Tris: 10 mM, NaCl: 50 mM, pH 7.6, Sigma-Aldrich) unless specified. DNA sequences

were designed with Oligo Analyzer (Integrated DNA Technologies, Inc., Coralville, IA) to minimize secondary structures. Single-stranded 60-bp DNA molecules were synthesized by IBA GmbH (Goettingen, Germany), and single-stranded 20-bp and 40-bp DNA molecules were synthesized by IDT, Inc. (Coralville, IA). All single-stranded DNA (ssDNA) molecules were purified with high-performance liquid chromatography (HPLC) after synthesis. For the purpose of immobilization, ssDNA molecules were modified with amine-C6 linkers on the 5' or 3' end. Fluorophores Atto647N or Atto532 were labeled on the other end of the amino-modified strand or on the 5' or 3' end of the complementary strand. The DNA sequences and modifications used in different experiments are shown in Table S1 of Supplementary Information. The dsDNA molecules were hybridized at 30 μM in 150 mM sodium phosphate buffer (prepared with sodium phosphate monobasic and sodium phosphate bibasic, pH 8.5, Sigma-Aldrich) before spotting. Microarray substrates were prepared from silicon wafers that had 17.5 μm thick thermally grown oxide (Silicon Valley Microelectronics, Santa Clara, CA), which were cut into 15 mm × 15 mm square chips. Before use, chips were rinsed with acetone, methanol, subjected to sonication in acetone for 5 min, and oxygen plasma ashing (M4LTM, PVA TePla America, Corona, CA) for 10 min.

DNA microarray and polymeric coating preparation: Clean chips were functionalized with a commercial polymer product MCP-2 from Lucident Polymers (Sunnyvale, CA), which will be referred to as the polymer). The polymer is obtained from radical copolymerization of *N,N*-dimethylacrylamide(DMA), *N*-acryloyloxysuccinimide(NAS), and 3-(trimethoxysilyl)-propyl methacrylate (MAPS), and covalently binds to amino-modified DNA as described elsewhere[35,46]. The polymer has been shown to have many advantages for DNA immobilization, such as high stability and reproducibility, fast and cost-effective preparation procedures, and minimal non-

specific binding[32,35,47]. The chips were immersed in a 1:1 mixture of 1% (w/v) MCP-2 in DI water and ammonium sulfate at 40% saturation concentration for 30 min, subsequently washed thoroughly with DI water, dried with argon gas, and then baked for 15 min at 80°C. DNA molecules were spotted in micro-arrayed fashion in 150 mM sodium phosphate (pH 8.5) buffer using a robotic spotter (sciFLEXARRAYER, Scienion, Monmouth Junction, NJ), and then immobilized for twelve hours in 65% humidity at room temperature. The chips were then washed on an orbital shaker three times in 2x saline-sodium citrate buffer (SSC) for 10 minutes, three times in 0.2x SSC for 5 minutes, once in 0.1x SSC for 1 minute, dried with argon gas, and kept in vacuum until measurements were performed. The diameter of each individual DNA spot was about 150 μm. Low background and consistent spot morphology were previously shown for DNA microarrays on glass slides functionalized with the polymer. DNA spot morphology was optimized by changing spotting conditions, such as concentration, temperature and humidity, and examined with a fluorescence scanner before measurements. Within the measured area at the center of the DNA spots, all spots possessed satisfactory uniform morphology (Supplementary Information, Section 2).

Measurements in a customized flow cell: Both DNA orientation and hybridization measurements were performed in a customized flow cell, where the chip surface was incubated in buffer (Supplementary Information, Section 3). A silicone rubber sheet (McMaster-Carr, Robbinsville, NJ), a glass window (Edmund Optics, Barrington, NJ), and the flow cell bottom formed the flow chamber, which were clamped and sealed using four screws. The custom-made glass window has anti-reflection coatings in the visible and near-infrared spectrum specific for each side so as not to affect spectral signals. The working volume of the flow cell was 100 μL. Buffer solutions were filtered with 0.1 μm Millex-LG syringe filter (Millipore, Billerica, MA)

before introduction to remove impurities. A peristaltic pump (Control Company, Friendswood, TX) drove buffer at a constant flow rate of 240 μL/min. The flow cell was fixed onto a 2-axis positioning micro-stage (Mad City Labs, Madison, WI), and the scanning of the DNA microarray was implemented by moving the stage by the DNA spot center-to-center distance with sub-micrometer accuracy.

Optical setup (Figure 3): The light beams of a red laser (helium-neon, 633 nm, Melles Griot, Carlsbad, CA) and a green laser (diode-pumped solid-state, 532 nm, Laserglow Technologies, Toronto, Canada) were combined with a dichroic beamsplitter. The combined laser beams were collimated, and expanded with two achromatic lenses (Thorlabs Inc., Newtown, NJ). A mechanical shutter that opens and closes via a transit TTL signal (+5V or 0V) controlled the red laser. A current control module regulated the green laser upon receiving a TTL signal (+5V or 0V). A printed circuit board (PCB) was designed to receive digital signals from the computer and send TTL signals to the shutter and the controller. The laser beams were then reflected by a dual-edge dichroic beam splitter (545/650 nm BrightLine, Semrock, Inc. NY), which specifically reflects the wavelengths of both lasers and transmits over 90% of the emission spectrums of the two fluorophores. A Nikon 5x objective with a numerical aperture (NA) of 0.13 focused the laser beams to diffraction-limited spots at the center of each DNA spot on the sensor surface. Emitted fluorescence was collected by the objective and focused onto a spectrometer connected to a CCD camera (SP-2150i, Princeton Instruments, Trenton, NJ). A yellow LED (M565L2, Thorlabs, Newton, NJ) was used as the illumination source for LED-RS measurements. A pinhole with a diameter of 100 μm was placed in front of the LED and a reduced image of the pinhole was focused to the same location as the laser spots. The reflected LED light was then collected and focused onto the spectrometer with the same focus as the laser beams. The spectrometer, the

micro-stage, and the lasers were controlled via custom MATLAB software that performs automatic data acquisition. The interference spectrums consisted of three parts: the fluorophore or the LED emission spectral envelope, the oscillatory interference component, and the shot noise collected from the CCD camera. Both fluorescence and LED interference spectrums were fit with custom algorithms to obtain fluorophore heights and bio-layer thicknesses as described elsewhere[48].

Calculation of dsDNA orientation using fluorophore height measurements: The average orientation of dsDNA was calculated by applying simple trigonometry using the fluorophore height difference (Δh) and the end-to-end length of the dsDNA. The persistence length (l) of dsDNA is approximately 50 nm in our buffer solutions[49]. Thus a short dsDNA molecule (<150bp) can be modeled as a rigid rod tethered to the sensor surface. The length of the rod is defined by the root-mean-square (rms) end-to-end distance ($\sqrt{\langle r^2 \rangle}$) of the dsDNA based on the worm-like chain model[50]. Therefore, the average orientation of dsDNA relative to the surface is $\langle \theta \rangle = \arcsin\left(\langle \Delta h \rangle / \sqrt{\langle r^2 \rangle}\right)$, where $\langle \Delta h \rangle$ is ensemble average of the fluorophore height difference between the surface-distal and surface-proximal ends of the dsDNA molecules resided within the measured area (Supplementary Information, Section 5).

Quantification of DNA surface density: The DNA layer thickness measured by LED-RS and a calibration coefficient (1ng/mm^2/nm)[40,51] were used to calculate the DNA mass surface density. Furthermore, using the DNA molecular weight and the Avogadro constant, the molecular surface density can be calculated from the mass surface density. For example, a 1nm thick dsDNA spot (60-bp, molecular weight: 38700g/mol) renders a molecular surface density of 1.56×10^{12} molecules/cm^2.

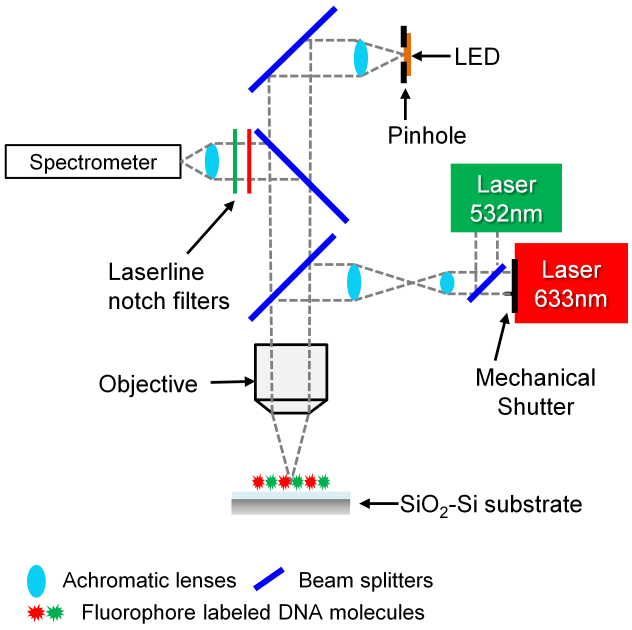

Figure 3 Schematic illustration of the optical setup combining the dual-color SSFM and WLRS using a LED as illumination source (referred to as LED-RS). Components of the system shown are not to scale.

3. Results and discussion

Design of the SiO_2 layer thickness and validation of dual-color SSFM and LED-RS. Employing the interference spectrum at two different spectral ranges by dual-color SSFM and LED-RS on the same chip requires us to use substrates with a thicker SiO_2 layer. Previously for single-color SSFM using a substrate with 5 μm SiO_2 layer, at least two periods of oscillations that spanned a bandwidth of about 1000 cm^{-1} within the fluorescence emission spectrum were needed to precisely determine fluorophore axial heights with less than 1 nm deviation[52]. However, for the combined dual-color SSFM and LED-RS, the bandwidths usable for fitting without sacrificing signal-to-noise ratio were much narrower, constrained by the emission spectrums of the flourophores and the LED and the passbands of the available dichroic beam splitters and notch filters. Since the interference oscillation period is inversely proportional to the

thickness of the SiO_2 layer[36], within the narrower bandwidths, we need to use thicker SiO_2 layer to obtain sufficient oscillation periods for precise height determination. We simulated the fluorophore axial height deviation from expected values on substrates with different SiO_2 thicknesses under the available bandwidths in the system (red fluorophore: 700 cm^{-1}, green fluorophore: 450 cm^{-1}, LED: 800 cm^{-1}). Based on the simulation, we selected a substrate with 17.5 μm thick SiO_2 layer that allowed for at least two periods of oscillations within each spectral bandwidth used by dual-color SSFM and LED-RS (Supplementary Information, Section 4).

Table 1 shows that the fluorophore axial heights measured on the newly designed substrate utilizing a 17.5 μm SiO_2 layer by dual-color SSFM were as precise as traditional single-color SSFM. We spotted an array of 60-bp dsDNA with different modifications, measured the average height difference (Δh) between the surface-distal and surface proximal ends of the dsDNA, and calculated the dsDNA orientations to the surface (See Experimental Section). In Table 1, the schemes (a) and (b) represent single-color SSFM while schemes (c) and (d) represent dual-color SSFM. We also measured nanometer-scale steps etched on the SiO_2 surface by single-color SSFM, dual-color SSFM and LED-RS. The results show that all modalities can determine the nanometer axial height differences with comparable accuracy both in air and in solution (Supplementary Information, Section 6).

Table 1. Compare quantification of surface-immobilized dsDNA orientation in different detection schemes. Data presented is the mean and standard deviation of the height difference (Δh) between the surface-distal and surface-proximal ends of the dsDNA on 10 separate DNA spots or spot pairs.

Detection schemes	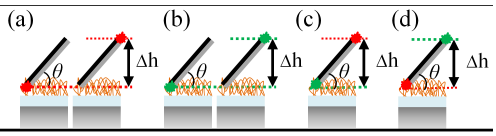					
	(a)		(b)		(c)	(d)
DNA name	Seq1	Seq2	Seq3	Seq4	Seq5	Seq6
$\langle \Delta h \rangle$(nm)	11.9		11.0		11.7	11.6
$SD_{\langle \Delta h \rangle}$	1.0		1.3		0.8	0.6
$\langle \theta \rangle$(°)	38.6		35.2		37.7	37.2
$SD_{\langle \theta \rangle}$	3.0		3.9		2.5	1.9

Characterization of the conformation of dsDNA immobilized on the polymer surface. We used dual-color SSFM combined with LED-RS to evaluate the effects of surface density, buffer ionic strength, and DNA length on the conformation of dsDNA on the polymer surface immersed in buffer solution. First, we observed that the orientation of dsDNA to the surface positively correlated to its surface density on the polymer surface. We measured an array of 60-bp fluorophore-labeled dsDNA immobilized at concentrations ranging from 8 μM to 10 μM to generate dsDNA spots of varied surface densities. We determined the surface densities of the dsDNA spots with LED-RS and their ensemble average orientations with dual-color SSFM. For SSFM measurements, DNA spots of different surface densities were exposed for different lengths of time, ranging from 0.1 second to 1 second. The dual-color SSFM optical setup operates in the shot noise limited regime where the signal-to-noise ratio (SNR) is proportional to the square root of signal counts. The exposure time was selected to ensure sufficient signal counts, corresponding to at least a SNR of 30 for accurate fitting and axial localization. Figure 4(a) shows that dsDNA orientation has a positive correlation with surface density. This correlation was expected because as the density of dsDNA layer increased, the distance between adjacent dsDNA molecules became smaller, resulting in stronger electrostatic repulsion and more steric hindrance between the dsDNA molecules. As illustrate in Figure 4(d), the random

rotational freedom for each dsDNA molecule under thermal fluctuation decreased, and thus the ensemble average orientation of the dsDNA from the surface increased.

The measured orientations of dsDNA shown in Figure 4(a) were lower than the values predicted by trigonometric calculations using a rigid rod model of dsDNA on a 2-D surface, which are over 76° to the surface, much higher than our results. We attribute this discrepancy to the 3-D geometry of the polymer surface. The actual distance between the dsDNA molecules were presumably larger than that calculated based on 2-D surface geometry. The polymeric coating swells by about 7 to 20 nm upon hydration and its functional groups for immobilization are distributed in the axial dimension[32,35]. As a result, the dsDNA molecules may penetrate the polymer scaffold and also be distributed axially depending on the polymer pore size and the dsDNA length. Hence, the axial penetration and distribution of the dsDNA molecules resulted in reduced ensemble average height differences between surface-distal and surface–proximal ends, and consequently reduced average orientations. Moreover, axial distribution of the immobilized dsDNA molecules potentially added more space for random rotation, which could also lead to lower calculated orientations compared to those based on a 2-D surface model.

Next, we examined the effects of buffer ionic strength on the orientation of 60-bp dsDNA molecules by measuring the average orientation of 10 dsDNA spot replicates in buffers of different NaCl concentrations (Figure 4(b)). We observed that average orientation of dsDNA on the polymer surface negatively correlated to the buffer ionic strength, which agrees with Manning's counterion condensation theory[53]. The theory states that cations in the buffer can condense onto the negatively charged dsDNA backbones. Therefore, increased concentration of cations in the buffer shielded the electrostatic repulsive forces between the dsDNA molecules, which resulted in more random rotational freedom of the dsDNA and therefore lowered the

average orientation. Figure 4(b) shows that when the salt concentration was sufficiently high, the effect of the electrostatic repulsion between dsDNA molecules on their orientation became minimal. The orientation of 60-bp dsDNA molecule approached 33°, the statistical average orientation of dsDNA with full random rotation freedom under thermal fluctuations on a 2-D surface (Supplementary Information, Section 5). However, the intermolecular distance calculated from the surface density was about 6.8 nm, where the DNA molecules should be sterically restricted from random free rotation. This observation again implied that under the same surface density used in the measurement, the dsDNA molecules had more free rotational space on the 3-D polymer surface than on a 2-D surface.

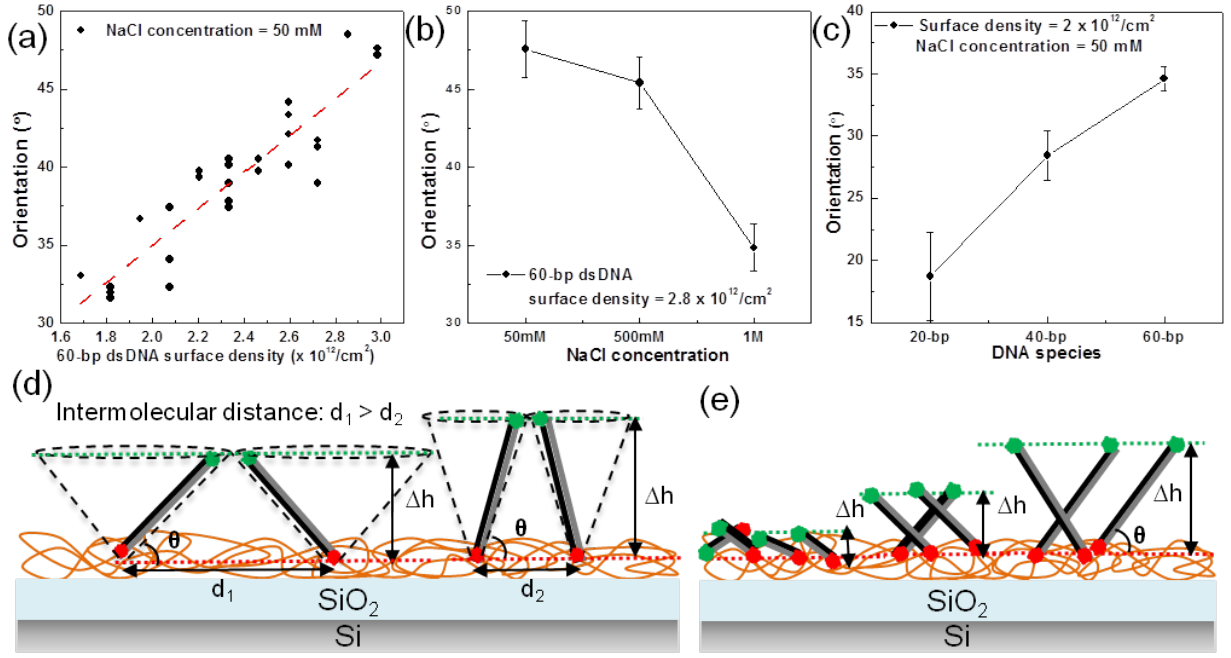

Figure 4 Characterization of DNA molecules immobilized on a polymeric surface. Error bar shows standard deviation of 10 dsDNA spots. (a) The average orientation of each dsDNA spot positively correlates to its surface density. The red dashed line is a guide to the eye. (b) The orientation of dsDNA negatively correlates to buffer ionic strength. (c) Long dsDNA spots have larger average orientations than those of short dsDNA spots on the polymer surface. (d)

Schematic illustration of the effect of surface density on the orientation of dsDNA. (e) Short dsDNA molecules may penetrate the polymeric surface and orient downtowards, resulting in lower average orientation.

Finally, by measuring orientations of three dsDNA species of different lengths, we provide evidence that shorter dsDNA molecules have more freedom of random thermal rotations on the polymer surface. 20-bp, 40-bp, and 60-bp dsDNA spots were immobilized of the same surface density and measured in buffer of the same NaCl concentration. Figure 4(c) shows that the average orientation of longer dsDNA molecules was larger than that of shorter dsDNA molecules. This trend was anticipated since shorter dsDNA molecules, when immobilized at a similar density, have less steric hindrance and electrostatic repulsion between them than longer dsDNA molecules. However, the average orientation of 20-bp dsDNA was smaller than the statistical average (33°) of dsDNA freely rotating on a planar surface[54]. The length of 20-bp dsDNA (~6.5 nm) is comparable to the diameter of the polymeric pore size (~5 nm) in hydrated state[32]. Hence as illustrated in Figure 4(e) the 20-bp dsDNA may orient downwards in the 3-D polymer surface. The result indicates that short dsDNA of length comparable to the polymeric pore size can have 3-D random rotational freedom when the polymer is hydrated and swells.

Real-time quantification of conformational change and binding during DNA hybridization on the polymer surface. We demonstrate the use of dual-color SSFM and LED-RS for simultaneous quantification of DNA conformational change and complementary strand binding during DNA surface hybridization. We immobilized 60-bp ssDNA modified with amine-C6 linker at the 3' end (surface-proximal end) and the red fluorophore at the 5' end (surface-distal end) on a polymer-functionalized chip. The chip was fixed in a customized flow cell with its surface immersed in buffer solution, which was driven by a peristaltic pump (Supplementary

Information, Section 3). After flowing only hybridization buffer for a baseline measurement, we introduced hybridization buffer containing complementary strands at a concentration of 500 nM at 45 °C. The surface-distal red fluorophore height and the thickness of the ssDNA layer were monitored at a time interval of 21 seconds before and during hybridization while the proximal green fluorophore height was measured after hybridization reached equilibrium. The time resolution was set so that over 100 fluorescence measurements were taken during the entire hybridization process before the fluorophores became completely photobleached.

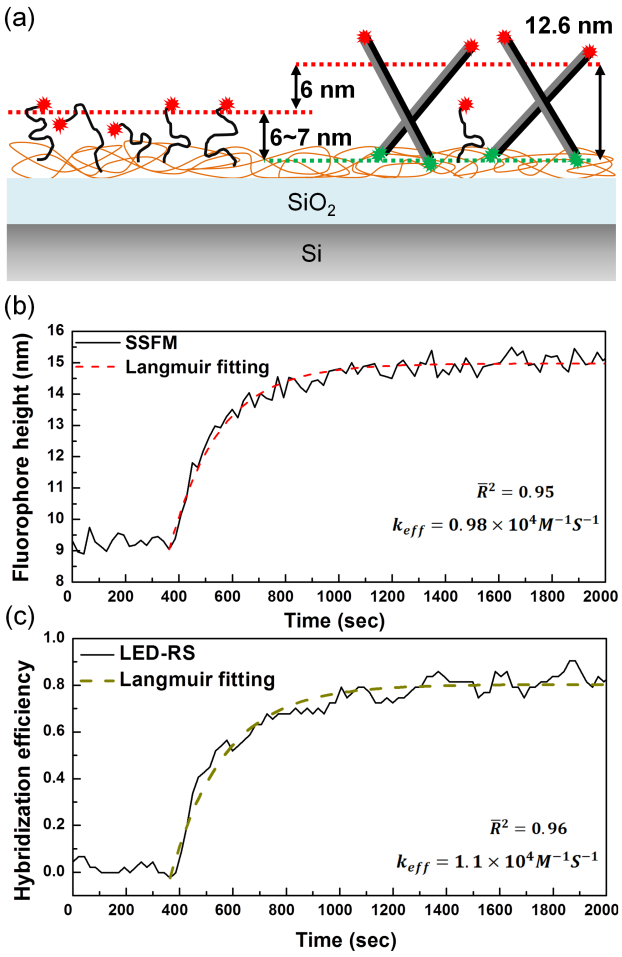

Figure 5 Real-time detection and quantification of DNA conformation and hybridization using dual-color SSFM and LED-RS. (a) Schematic illustration of the DNA hybridization process on the polymer surface. Average fluorophore heights are indicated as dotted lines. (b) Hybridization

efficiency calculated from the fraction of additional thicknesses of the DNA spot measured by LED-RS with a time resolution of 21 seconds. (c) Simultaneous detection of the average height increase of the red fluorophores at the surface-distal end of the ssDNA probes during hybridization. A first-order Langmuir kinetic equation was fit to both measurements and both observed effective rate constants around $1\times10^4\ M^{-1}S^{-1}$.

The average height of the distal red fluorophores increased from 9 nm to about 15 nm and the average thickness of the DNA layer increased from 1.5 nm to 2.7 nm as ssDNA became hybridized into dsDNA till binding equilibrium was reached (Figure 5). The initial thickness of the ssDNA layer corresponded to an immobilization density of 3.8×10^{12} cm^{-2}. The DNA hybridization efficiency was 0.8 at steady state obtained by calculating the fraction of additional thickness on the surface. Based on the studies of DNA hybridization regimes by Levicky and Melosh[20,55], the surface density under our experimental condition was in the pseudo-Langmuir regime (2×10^{12} cm^{-2} to 6×10^{12} cm^{-2}). We thus fit each dynamic hybridization data to the first-order Langmuir kinetic equation (Figure 5):

$$x = X_{eq}(1 - e^{-k_{eff}C_t t})$$

For LED-RS measurement, x denotes the hybridization efficiency, and X_{eq} is the steady state hybridization efficiency. For SSFM measurement, x denotes the average ensemble red fluorophore height at the surface-distal end of the ssDNA, and X_{eq} is the average ensemble red fluorophore height at steady state. For both measurements, k_{eff} is the effective rate constant, C_t is the concentration of the target complementary strands, and t is time. The k_{eff} of DNA spot mass density change, indicated by the hybridization efficiency change, and DNA conformation change, indicated by the red fluorophore height change, were both around $1\times10^4\ M^{-1}S^{-1}$.

The height increase at the surface-distal end of the ssDNA probes signified that the DNA conformation changed from highly flexible single-stranded coils to rigid double-stranded helices (Figure 5(a)). The average fluorophore height increase was approximately 6 nm (Figure 5(b)), which agrees with the displacement range between 3 and 10 nm determined by a single-molecule micromechanical method[56]. The complementary strands had green fluorophores tagged to the 5' end, which resided on the surface-proximal end of the immobilized ssDNA molecules upon hybridization. After hybridization reached equilibrium, we replaced the hybridization solution in the flow cell with pure buffer and measured the height of the green fluorophores at about 2 to 3 nm. If we subtract the average height of the green fluorophores from that of the red fluorophores, we then obtained the height difference between the surface-distal and surface-proximal ends of the ssDNA molecules before hybridization, which was about 6 to 7 nm as shown in Figure 5(a). ssDNA is often modeled as random coils in solution[57,58], whose flexibility is characterized by a persistence length of about 1 to 4 nm. This larger than persistence length height difference implies that rather than a complete random coil, the immobilized ssDNA molecules had an extended conformation on the polymer surface. This extended conformation was also observed on short ssDNA tethered to a 2-D gold surface[25].

Figure 5(b) shows that the DNA hybridization efficiency at equilibrium was smaller than one. Many factors can affect the efficiency of DNA surface hybridization[20]. We first attribute to the electrostatic barrier created by the DNA layer negative potential, which was enhanced along the incorporation of more negatively charged complementary strands. Moreover, hybridized dsDNA and the polymeric surface might also sterically hinder the incorporation of the complementary strands. The hybridization efficiency can be improved by both lowering the surface density and increasing the buffer ionic strength[20].

We demonstrated the implementation of a dual-color SSFM combined with LED-RS for the nanoscale characterization of DNA conformation on a 3-D polymer surface. The system improved upon traditional single-color SSFM and white light reflectance spectrometry by using a substrate with a thicker SiO_2 layer (17.5 μm) and a LED illumination source. The newly designed substrate along with additional optical components enabled the use of multiple spectral bandwidths for precise axial localization of two different fluorophores and quantification of DNA surface density. We note that SSFM determines the axial location of fluorophores from the spectral oscillations, not from fluorescence intensity variations. Thus experimental conditions that can potentially cause fluorescence intensity variations do not affect the results.

Our results demonstrate that dual-color SSFM is advantageous over traditional single-color SSFM. For example, DNA surface density affects the orientation of surface-immobilized DNA. Previously, single-color SSFM determined orientations of surface-immobilized dsDNA by measuring the height differences between surface-distal and surface-proximal ends on separate DNA spots, which might have different immobilization densities and axial distributions. Also, dual-color SSFM increases the throughput of the height measurements under limited number of arrayed spots. Additionally, dual-color SSFM offers new assay designs. For instance, the location of one fluorophore tagged to a DNA-binding protein can be compared to another labeled at a reference location on the DNA molecule to determine the protein binding site along the DNA sequence. Comparing to fluorescence resonance energy transfer (FRET)[59], dual-color SSFM does not require a complex fluorescence normalization procedure in spectrum processing. Moreover, the axial heights measurable using dual-color SSFM ranges from subnanometer to more than 100 nanometers[36] (Supplementary Information, Section 7) whereas the distance measurable using FRET is less than 10 nm[59]. Comparing to acoustic wave sensors, the results of

dual-color SSFM are directly interpreted as the geometric features of DNA conformation rather than mechanical properties of DNA films, such as modulus and viscosity[60]. Moreover, LED-RS provides orthogonal information of the DNA surface density, which is often coupled with the signal generated by DNA conformational change for mechanical and optical resonance based sensors. Notably, the nanoscale DNA conformational change from flexible coils to rigid double helices was simultaneously monitored during the addition of complimentary sequence to ssDNA probes.

Our results of the orientation and surface density of dsDNA molecules indicated that dsDNA immobilized on a 3-D polymeric coating have more random rotation freedom under thermal fluctuations than those immobilized on a 2-D surface in hydrated environment. A precise model describing the relationship between the average orientation and surface density is unattainable at the moment due to lack of the exact axial distribution of dsDNA molecules using average ensemble measurements. Yet our results suggested that this larger degree of free random thermal rotation of the DNA molecules, and possibly of protein molecules, could cause the previously described high performance of the polymeric coating, such as high surface density, bioactivity retaining, and easy accessibility of the immobilized molecular probes[35,47].

Although dual-color SSFM and LED-RS allowed for real-time simultaneous quantification of molecular binding and conformational change, a few limitations need to be overcome in future developments. First, other fluorescence labels with narrow spectrums, such as Quantum Dots (QDs) should be used to replace the fluorophores for real-time measurements. In this work, the green and red fluorescence spectrums were measured separately. The tail of the green fluorophore emission spectrum overlapped with that of the red fluorophore, which can affect the accuracy of red flurophore localization if measured at the same time. Therefore, during DNA

hybridization, we only measured the green fluorophore height after hybridization reached steady state in pure buffer without complementary sequences. Moreover, the fluorophores photobleach after limited number of measurements, limiting the time resolution for monitoring real-time binding processes. Also, FRET occurred between green fluorophores and the red flurophores, and expedited the photobleaching of red fluorophores. Non-blinking quantum dots (QDs)[61] possessing narrow non-overlapping spectrums can be a good substitute. The emission of QDs can be excited at the same laser wavelength and they have extraordinary brightness and photostability as compared to organic fluorophores, which have already been exploited in cell imaging and biological sensing[62]. Second, the flow cell employed for real-time hybridization measurements operated in a diffusion-limited regime[63]. Thus, the observed effective rate constants of DNA binding and conformational change were indistinguishable, both of which were limited by the transportation rate of the complementary strands to the surface-immobilized ssDNA. Thus, the flow cell needs to be optimized to a reaction-limited regime, where the rates of conformational change and binding can help determine the biophysical mechanisms of the reaction. Additionally, the current optical setup is configured in a point-to-point scanning modality where only one DNA spots can be measured at a time. A 2-D spectral imaging modality using spatial line scanning are currently being implemented to image and measure an array of DNA spots simultaneously. This spectral imaging modality can dramatically improve the measurement throughput and reduce the time resolution for measuring an array of DNA spots in real-time assays.

4. Conclusion

In summary, we have demonstrated the development of a dual-color SSFM combined with independent biomolecular sensing for the characterization of nanoscale conformation of DNA on

a 3-D polymer surface. A newly designed substrate with a thick SiO_2 layer (17.5 μm) allowed for the use of multiple spectral bandwidths for precise axial localization of two different fluorophores and quantification of biomolecule surface density. Using dual-color SSFM, we have shown that the conformation of surface-immobilized dsDNA on a 3-D polymeric surface was subject to surface density, buffer ionic strength, and dsDNA length. Furthermore, dsDNA immobilized on a polymeric surface possess more conformational freedom than those on a 2-D surface, providing additional evidence for the high density and easy accessibility of biomolecules on 3-D polymeric coating in molecular binding assays. Particularly, we have shown simultaneous and independent real-time monitoring of DNA conformational change and complementary strand binding during DNA surface hybridization. The overall optical setup is simple and compatible with regular fluorescence microscopes. All measurements were performed in a flow cell on DNA microarrays, compatible with multiplexed parallel molecular binding assays. The versatility, simplicity, and robustness of the presented platform make it a useful tool that can be broadly used for quantitative nanoscale characterization of solid-biochemical interfaces for the optimization of various DNA sensors and nanodevices.

Electronic Supplementary Information (ESI) available: 1. Oligonucleotide sequences and nomenclature. 2. Uniform and consistent spot morphology of DNA microarrays on the polymer surface. 3. Schematic illustration of customized flow cell assembly. 4. Simulation of the deviation of fluorophore axial heights from expected values on substrates with different SiO_2 thicknesses. 5. Calculation of the average orientation of surface-immobilized dsDNA. 6. Validating the dual-color SSFM system with nanometer scale surface steps. 7. Simulation of the deviation of axial step heights from expected values using dual-color SSFM.

Acknowledgements

The authors would like to acknowledge National Science Foundation (Grant 0933670) for funding support. Xirui Zhang would like to thank Professor Bennett Goldberg for fruitful discussions during manuscript preparation.

References

1. Abel, G. R., Jr.; Josephs, E. A.; Luong, N.; Ye, T. A Switchable Surface Enables Visualization of Single DNA Hybridization Events with Atomic Force Microscopy. *J. Am. Chem. Soc.* **2013**, *135*, 6399–6402.
2. Wickham, S. F. J.; Bath, J.; Katsuda, Y.; Endo, M.; Hidaka, K.; Sugiyama, H.; Turberfield, A. J. A DNA-Based Molecular Motor That Can Navigate a Network of Tracks. *Nature Nanotechnology* **2012**, *7*, 169–173.
3. Plaxco, K. W.; Soh, H. T. Switch-Based Biosensors: a New Approach Towards Real-Time, in Vivo Molecular Detection. *Trends in Biotechnology* **2011**, *29*, 1–5.
4. Mao, Y.; Liu, D.; Wang, S.; Luo, S.; Wang, W.; Yang, Y.; Ouyang, Q.; Jiang, L. Alternating-Electric-Field-Enhanced Reversible Switching of DNA Nanocontainers with pH. *Nucleic Acids Research* **2007**, *35*, e33–e33.
5. Rant, U.; Arinaga, K.; Scherer, S.; Pringsheim, E.; Fujita, S.; Yokoyama, N.; Tornow, M.; Abstreiter, G. Switchable DNA Interfaces for the Highly Sensitive Detection of Label-Free DNA Targets. *Proceedings of the National Academy of Sciences* **2007**, *104*, 17364–17369.
6. Shu, W.; Liu, D.; Watari, M.; Riener, C. K.; Strunz, T.; Welland, M. E.; Balasubramanian, S.; McKendry, R. A. DNA Molecular Motor Driven Micromechanical Cantilever Arrays. *J. Am. Chem. Soc.* **2005**, *127*, 17054–17060.
7. Drummond, T. G.; Hill, M. G.; Barton, J. K. Electrochemical DNA Sensors. *Nature Biotechnology* **2003**, *21*, 1192–1199.
8. Hoheisel, J. D. Microarray Technology: Beyond Transcript Profiling and Genotype Analysis. *Nature Reviews Genetics* **2006**, *7*, 200–210.
9. Berger, M. F.; Bulyk, M. L. Universal Protein-Binding Microarrays for the Comprehensive Characterization of the DNA-Binding Specificities of Transcription Factors. *Nat Protoc* **2009**, *4*, 393–411.
10. FRCPath, P. J. S. R.-F.; MD, P. L. P. Gene Expression Profiling in Breast Cancer: Classification, Prognostication, and Prediction. *The Lancet* **2011**, *378*, 1812–1823.
11. Vallée-Bélisle, A.; Ricci, F.; Uzawa, T.; Xia, F.; Plaxco, K. W. Bioelectrochemical Switches for the Quantitative Detection of Antibodies Directly in Whole Blood. *J. Am. Chem. Soc.* **2012**, *134*, 15197–15200.
12. Bonham, A. J.; Hsieh, K.; Ferguson, B. S.; Vallée-Bélisle, A.; Ricci, F.; Soh, H. T.; Plaxco, K. W. Quantification of Transcription Factor Binding in Cell Extracts Using

an Electrochemical, Structure-Switching Biosensor. *J. Am. Chem. Soc.* **2012**, *134*, 3346–3348.

13. Farjami, E.; Clima, L.; Gothelf, K.; Ferapontova, E. E. "Off−on" Electrochemical Hairpin-DNA-Based Genosensor for Cancer Diagnostics. *Anal. Chem.* **2011**, *83*, 1594–1602.
14. Strohsahl, C. M.; Miller, B. L.; Krauss, T. D. Preparation and Use of Metal Surface-Immobilized DNA Hairpins for the Detection of Oligonucleotides. *Nat Protoc* **2007**, *2*, 2105–2110.
15. Josephs, E. A.; Ye, T. Nanoscale Spatial Distribution of Thiolated DNA on Model Nucleic Acid Sensor Surfaces. *ACS Nano* **2013**, *7*, 3653–3660.
16. Yu, Z.-G.; Lai, R. Y. Effect of Signaling Probe Conformation on Sensor Performance of a Displacement-Based Electrochemical DNA Sensor. *Anal. Chem.* **2013**, *85*, 3340–3346.
17. Pinheiro, A. V.; Nangreave, J.; Jiang, S.; Yan, H.; Liu, Y. Steric Crowding and the Kinetics of DNA Hybridization Within a DNA Nanostructure System. *ACS Nano* **2012**, *6*, 5521–5530.
18. Mirmomtaz, E.; Castronovo, M.; Grunwald, C.; Bano, F.; Scaini, D.; Ensafi, A. A.; Scoles, G.; Casalis, L. Quantitative Study of the Effect of Coverage on the Hybridization Efficiency of Surface-Bound DNA Nanostructures. *Nano Lett.* **2008**, *8*, 4134–4139.
19. Castronovo, M.; Radovic, S.; Grunwald, C.; Casalis, L.; Morgante, M.; Scoles, G. Control of Steric Hindrance on Restriction Enzyme Reactions with Surface-Bound DNA Nanostructures. *Nano Lett.* **2008**, *8*, 4140–4145.
20. Gong, P.; Levicky, R. DNA Surface Hybridization Regimes. *Proceedings of the National Academy of Sciences* **2008**, *105*, 5301–5306.
21. Marotta, N. E.; Beavers, K. R.; Bottomley, L. A. Limitations of Surface Enhanced Raman Scattering in Sensing DNA Hybridization Demonstrated by Label-Free DNA Oligos as Molecular Rulers of Distance-Dependent Enhancement. *Anal. Chem.* **2013**, *85*, 1440–1446.
22. Papadakis, G.; Tsortos, A.; Bender, F.; Ferapontova, E. E.; Gizeli, E. Direct Detection of DNA Conformation in Hybridization Processes. *Anal. Chem.* **2012**, *84*, 1854–1861.
23. Rezek, B.; Shin, D.; Uetsuka, H.; Nebel, C. E. Microscopic Diagnostics of DNA Molecules on Mono-Crystalline Diamond. *phys. stat. sol. (a)* **2007**, *204*, 2888–2897.
24. Wang, K.; Goyer, C.; Anne, A.; Demaille, C. Exploring the Motional Dynamics of End-Grafted DNA Oligonucleotides by in Situ Electrochemical Atomic Force Microscopy. *J. Phys. Chem. B* **2007**, *111*, 6051–6058.
25. Rant, U.; Arinaga, K.; Fujita, S.; Yokoyama, N.; Abstreiter, G.; Tornow, M. Structural Properties of Oligonucleotide Monolayers on Gold Surfaces Probed by Fluorescence Investigations. *Langmuir* **2004**, *20*, 10086–10092.
26. Patole, S. N.; Pike, A. R.; Connolly, B. A.; Horrocks, B. R.; Houlton, A. STM Study of DNA Films Synthesized on Si(111) Surfaces. *Langmuir* **2003**, *19*, 5457–5463.
27. Petrovykh, D. Y.; Kimura-Suda, H.; Tarlov, M. J.; Whitman, L. J. Quantitative Characterization of DNA Films by X-Ray Photoelectron Spectroscopy. *Langmuir* **2004**, *20*, 429–440.
28. Petrovykh, D. Y.; Kimura-Suda, H.; Whitman, L. J.; Tarlov, M. J. Quantitative

Analysis and Characterization of DNA Immobilized on Gold. *J. Am. Chem. Soc.* **2003**, *125*, 5219–5226.

29. Barhoumi, A.; Zhang, D.; Halas, N. J. Correlation of Molecular Orientation and Packing Density in a dsDNA Self-Assembled Monolayer Observable with Surface-Enhanced Raman Spectroscopy. *J. Am. Chem. Soc.* **2008**, *130*, 14040–14041.
30. Yang, Z.; Chevolot, Y.; Géhin, T.; Dugas, V.; Xanthopoulos, N.; Laporte, V.; Delair, T.; Ataman-Önal, Y.; Choquet-Kastylevsky, G.; Souteyrand, E.; *et al.* Characterization of Three Amino-Functionalized Surfaces and Evaluation of Antibody Immobilization for the Multiplex Detection of Tumor Markers Involved in Colorectal Cancer. *Langmuir* **2013**, *29*, 1498–1509.
31. Rendl, M.; Bönisch, A.; Mader, A.; Schuh, K.; Prucker, O.; Brandstetter, T.; Rühe, J. Simple One-Step Process for Immobilization of Biomolecules on Polymer Substrates Based on Surface-Attached Polymer Networks. *Langmuir* **2011**, *27*, 6116–6123.
32. Yalçın, A.; Damin, F.; Ozkumur, E.; di Carlo, G.; Goldberg, B. B.; Chiari, M.; Ünlü, M. S. Direct Observation of Conformation of a Polymeric Coating with Implications in Microarray Applications. *Anal. Chem.* **2009**, *81*, 625–630.
33. Rusmini, F.; Zhong, Z.; Feijen, J. Protein Immobilization Strategies for Protein Biochips. *Biomacromolecules* **2007**, *8*, 1775–1789.
34. Suriano, R.; Levi, M.; Pirri, G.; Damin, F.; Chiari, M.; Turri, S. Surface Behavior and Molecular Recognition in DNA Microarrays fromN,N-Dimethylacrylamide Terpolymers with Activated Esters as Linking Groups. *Macromol. Biosci.* **2006**, *6*, 719–729.
35. Pirri, G.; Damin, F.; Chiari, M.; Bontempi, E.; Depero, L. E. Characterization of a Polymeric Adsorbed Coating for DNA Microarray Glass Slides. *Anal. Chem.* **2004**, *76*, 1352–1358.
36. Moiseev, L.; Cantor, C. R.; Aksun, M. I.; Dogan, M.; Goldberg, B. B.; Swan, A. K.; Ünlü, M. S. Spectral Self-Interference Fluorescence Microscopy. *J. Appl. Phys.* **2004**, *96*, 5311.
37. Moiseev, L.; Ünlü, M. S.; Swan, A. K.; Goldberg, B. B.; Cantor, C. R. DNA Conformation on Surfaces Measured by Fluorescence Self-Interference. *Proceedings of the National Academy of Sciences* **2006**, *103*, 2623–2628.
38. Kitsara, M.; Petrou, P.; Kontziampasis, D.; Misiakos, K.; Makarona, E.; Raptis, I.; Beltsios, K. Biomolecular Layer Thickness Evaluation Using White Light Reflectance Spectroscopy. *Microelectronic Engineering* **2010**, *87*, 802–805.
39. Petrou, P. S.; Ricklin, D.; Zavali, M.; Raptis, I.; Kakabakos, S. E.; Misiakos, K.; Lambris, J. D. Real-Time Label-Free Detection of Complement Activation Products in Human Serum by White Light Reflectance Spectroscopy. *Biosensors and Bioelectronics* **2009**, *24*, 3359–3364.
40. Ozkumur, E.; Yalçın, A.; Cretich, M.; Lopez, C. A.; Bergstein, D. A.; Goldberg, B. B.; Chiari, M.; Ünlü, M. S. Quantification of DNA and Protein Adsorption by Optical Phase Shift. *Biosensors and Bioelectronics* **2009**, *25*, 167–172.
41. Cao, C.; Zhang, J.; Wen, X.; Dodson, S. L.; Dao, N. T.; Wong, L. M.; Wang, S.; Li, S.; Phan, A. T.; Xiong, Q. Metamaterials-Based Label-Free Nanosensor for Conformation and Affinity Biosensing. *ACS Nano* **2013**, *7*, 7583–7591.
42. Watkins, H. M.; Vallée-Bélisle, A.; Ricci, F.; Makarov, D. E.; Plaxco, K. W.

Entropic and Electrostatic Effects on the Folding Free Energy of a Surface-Attached Biomolecule: an Experimental and Theoretical Study. *J. Am. Chem. Soc.* **2012**, *134*, 2120–2126.

43. Akkahat, P.; Mekboonsonglarp, W.; Kiatkamjornwong, S.; Hoven, V. P. Surface-Grafted Poly(Acrylic Acid) Brushes as a Precursor Layer for Biosensing Applications: Effect of Graft Density and Swellability on the Detection Efficiency. *Langmuir* **2012**, *28*, 5302–5311.
44. Xue, C.; Yonet-Tanyeri, N.; Brouette, N.; Sferrazza, M.; Braun, P. V.; Leckband, D. E. Protein Adsorption on Poly(N-Isopropylacrylamide) Brushes: Dependence on Grafting Density and Chain Collapse. *Langmuir* **2011**, *27*, 8810–8818.
45. Sanavio, B.; Scaini, D.; Grunwald, C.; Legname, G.; Scoles, G.; Casalis, L. Oriented Immobilization of Prion Protein Demonstrated via Precise Interfacial Nanostructure Measurements. *ACS Nano* **2010**, *4*, 6607–6616.
46. Cretich, M.; Pirri, G.; Damin, F.; Solinas, I.; Chiari, M. A New Polymeric Coating for Protein Microarrays. *Analytical Biochemistry* **2004**, *332*, 67–74.
47. Cretich, M.; di Carlo, G.; Longhi, R.; Gotti, C.; Spinella, N.; Coffa, S.; Galati, C.; Renna, L.; Chiari, M. High Sensitivity Protein Assays on Microarray Silicon Slides. *Anal. Chem.* **2009**, *81*, 5197–5203.
48. Moiseev, L. Spectral Self-Interference Fluorescence Microscopy and Its Applications in Biology
. *Boston University Dissertation* **2003**.
49. Dobrynin, A. V. Electrostatic Persistence Length of Semiflexible and Flexible Polyelectrolytes. *Macromolecules* **2005**, *38*, 9304–9314.
50. Khokhlov, A. R.; Grosberg, A. Y.; Pande, V. S. *Statistical Physics of Macromolecules (Polymers and Complex Materials)*; 1994th ed. American Institute of Physics, 1997.
51. Gauglitz, G. Multiple Reflectance Interference Spectroscopy Measurements Made in Parallel for Binding Studies. *Rev. Sci. Instrum.* **2005**, *76*, 062224.
52. Dogan, M.; Yalcn, A.; Jain, S.; Goldberg, M. B.; Swan, A. K.; Ünlü, M. S.; Goldberg, B. B. Spectral Self-Interference Fluorescence Microscopy for Subcellular Imaging. *Selected Topics in Quantum Electronics, IEEE Journal of* **2008**, *14*, 217–225.
53. Manning, G. S. Limiting Laws and Counterion Condensation in Polyelectrolyte Solutions. v. Further Development of the Chemical Model. *Biophys. Chem* **1978**, *9*, 65–70.
54. Rant, U.; Arinaga, K.; Fujita, S.; Yokoyama, N.; Abstreiter, G.; Tornow, M. Electrical Manipulation of Oligonucleotides Grafted to Charged Surfaces. *Org. Biomol. Chem.* **2006**, *4*, 3448.
55. Wong, I. Y.; Melosh, N. A. An Electrostatic Model for DNA Surface Hybridization. *Biophysical Journal* **2010**, *98*, 2954–2963.
56. Singh-Zocchi, M.; Dixit, S.; Ivanov, V.; Zocchi, G. Single-Molecule Detection of DNA Hybridization. *Proceedings of the National Academy of Sciences* **2003**, *100*, 7605–7610.
57. Tinland, B.; Pluen, A.; Sturm, J.; Weill, G. Persistence Length of Single-Stranded DNA. *Macromolecules* **1997**, *30*, 5763–5765.
58. Murphy, M. C.; Rasnik, I.; Cheng, W.; Lohman, T. M.; Ha, T. Probing Single-

Stranded DNA Conformational Flexibility Using Fluorescence Spectroscopy. *Biophysj* **2004**, *86*, 2530–2537.

59. Hillisch, A.; Lorenz, M.; Diekmann, S. Recent Advances in FRET: Distance Determination in Protein–DNA Complexes. *Current Opinion in Structural Biology* **2001**, *11*, 201–207.

60. Tsortos, A.; Papadakis, G.; Mitsakakis, K.; Melzak, K. A.; Gizeli, E. Quantitative Determination of Size and Shape of Surface-Bound DNA Using an Acoustic Wave Sensor. *Biophysj* **2008**, *94*, 2706–2715.

61. Wang, X.; Ren, X.; Kahen, K.; Hahn, M. A.; Rajeswaran, M.; Maccagnano-Zacher, S.; Silcox, J.; Cragg, G. E.; Efros, A. L.; Krauss, T. D. Non-Blinking Semiconductor Nanocrystals. *Nature* **2009**, *459*, 686–689.

62. Medintz, I. L.; Uyeda, H. T.; Goldman, E. R.; Mattoussi, H. Quantum Dot Bioconjugates for Imaging, Labelling and Sensing. *Nat Mater* **2005**, *4*, 435–446.

63. Squires, T. M.; Messinger, R. J.; Manalis, S. R. Making It Stick: Convection, Reaction and Diffusion in Surface-Based Biosensors. *Nature Biotechnology* **2008**, *26*, 417–426.

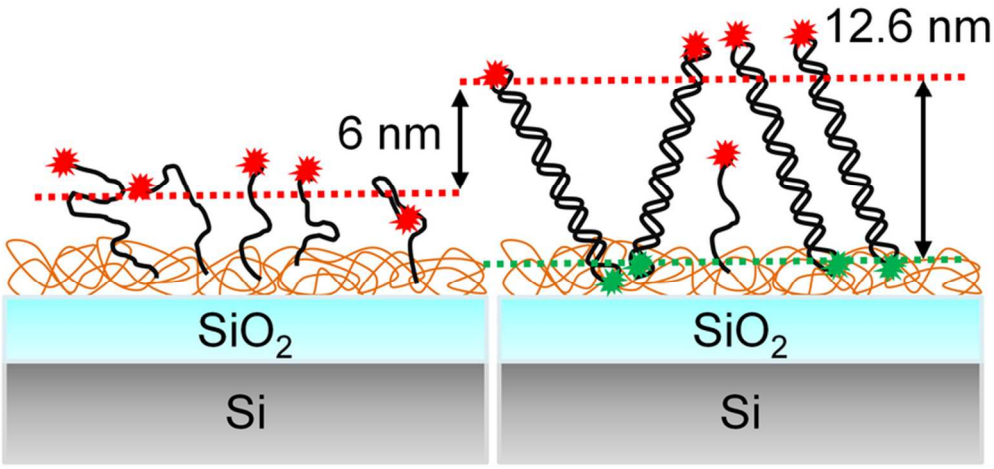

Simultaneous quantification of surface density and conformation of surface-immobilized DNA on a layered substrate functionalized with 3-D polymeric coating.
38x18mm (600 x 600 DPI)